Editors' Suggestion

Inhomogeneous disordering at a photoinduced charge density wave transition

Antonio Picano, Francesco Grandi,* and Martin Eckstein
Department of Physics, University of Erlangen-Nuremberg, Staudtstraße 7, 91058 Erlangen, Germany

(Received 16 April 2023; accepted 22 May 2023; published 7 June 2023)

Using ultrashort laser pulses, it has become possible to probe the dynamics of long-range order in solids on microscopic timescales. In the conventional description of symmetry-broken phases within time-dependent Ginzburg-Landau theory, the order parameter evolves coherently, with small fluctuations along an average trajectory. Recent experiments, however, indicate that some systems can support a different scenario, named ultrafast inhomogeneous disordering, where the average order parameter is no longer representative of the state on the atomic scale. Here we theoretically show that ultrafast disordering can occur in a minimal, yet paradigmatic, model for a Peierls instability if atomic scale inhomogeneities of both the electronic structure and the charge density wave order parameter are taken into account. The latter is achieved using a nonequilibrium generalization of statistical dynamical mean-field theory coupled to stochastic differential equations for the order parameter.

DOI: 10.1103/PhysRevB.107.245112

I. INTRODUCTION

Symmetry breaking phase transitions are among the most fundamental phenomena in physics, from cosmology to condensed matter. Understanding their dynamics in solids is therefore of basic interest as much as it is needed to establish pathways to control complex states of matter on ultrafast timescales [1,2]. The conventional phenomenological understanding of symmetry breaking is based on Ginzburg-Landau theory (GLT), which determines the order parameter from a free energy density. The latter depends on the electronic state through few variables like temperature, and it can therefore be rapidly modified by an excitation of the electrons. Time-dependent GLT has been successfully used to describe the resulting coherent dynamics of various orders, including superconductivity and charge density waves [3–9]. Nevertheless, in many experiments the dynamics of ordered phases comes with yet unresolved mysteries, including the emergence of metastable states which cannot be reached along equilibrium pathways [10–12] or dynamics which is not governed by the free energy for the measured electronic temperature [13].

A theoretical description beyond time-dependent GLT must properly include nonthermal order parameter fluctuations on various length and time scales. Including spatial fluctuations into time-dependent GLT in fact has a profound influence on the dynamics. For example, fluctuations of a thermodynamically subdominant order can become observable when the dominant order is transiently suppressed [14] and they can be important for a transition to metastable states [15]. Moreover, due to the anharmonicity of the potential, nonthermal fluctuations can renormalize the free energy. This can lead to a slowdown of the dynamics [16] or, in systems with discrete symmetry breaking, to a qualitative change of the potential [17]. Finally, even in the disordered phase, nonthermal order parameter fluctuations can leave characteristic signatures in the electronic properties [18–21].

In the above mentioned extensions of GLT, the order parameter is described by a homogeneous time-dependent mean $\phi_0(t)$, with small spatial fluctuations $\delta\phi(\vec{r},t)$ that are treated within a Gaussian approximation, i.e., the distribution of the fluctuations is assumed to be Gaussian around the average $\phi_0(t)$. An entirely different paradigm, which has been put forward in recent experimental studies [23–25], is ultrafast inhomogeneous disordering: in this scenario, the local configuration of the order parameter has a highly non-Gaussian distribution and is therefore no longer represented by its average $\phi_0(t)$. For example, in a discrete ($\mathbb{Z}_2$) symmetry-breaking transition, ultrafast inhomogeneous disordering could imply that the local order parameter shows a transient bimodal distribution peaked around large positive and negative displacements, say $\phi_0(t)+\Delta\phi$ and $\phi_0(t)-\Delta\phi$, respectively. In this case, its average $\phi_0(t)$ is not representative anymore of the distribution of the single displacements. Although this state cannot be distinguished from a Gaussian disordered state on the macroscopic level, by just looking at the average order parameter, its local microscopic nature is not captured by the Gaussian approximation, and one can expect a profoundly different dynamics. From a different perspective, this behavior corresponds to a temporary high density of atomic scale defects in the ordered state.

Inhomogeneous disordering also questions the conventional assumption that, after a short relaxation, electrons can be described by a few variables like the effective temperature and the excitation density. Along with the order parameter, in fact, also the local electronic structure may not be well represented by averaged spectra and distribution functions. Moreover, rapid electronic thermalization can be inhibited in disordered systems even in the presence of interactions, as for the case of many-body localization [26,27]. The intertwined evolution of the order parameter fluctuations and the electronic structure may lead to unusually slow relaxation, reminiscent of weak ergodicity breaking in translationally invariant systems due to dynamical bottlenecks and

*Corresponding author: grandi@physik.rwth-aachen.de

constraints [28–32]. A theoretical description of inhomogeneous disordering should therefore consider the possibility of a nonthermal and spatially varying electronic state, while previous simulations of dynamical symmetry breaking which start from a microscopic description of the electrons often neglect spatial fluctuations [33–36], with a recent exception [37].

With the current state of theory, even a minimal model to study inhomogeneous disordering should provide important insights. In the present work, we solve the coupled equations for the inhomogeneous order parameter evolution and the nonequilibrium electron dynamics in a minimal, yet paradigmatic model for a charge ordering transition, i.e., the Holstein model on the infinitely coordinated Bethe lattice. We find that already this simple model supports an inhomogeneous disordering scenario, which suggests that such self-generated disorder might more generally be of importance for the photoinduced dynamics in solids. Our model also allows one to investigate experimentally relevant aspects of that state, in particular the in-gap spectral weight and the slow recovery dynamics.

The article is structured as follows. In Sec. II, we introduce the Holstein model and the approach we developed to take into account nonequilibrium fluctuations of the order parameter. Section III presents both equilibrium results and nonequilibrium simulations after a photoexcitation. In Sec. IV, we reconstruct some out of equilibrium features of the potential energy, i.e., the potential energy barrier, without any original assumption on its existence. Finally, Sec. V is devoted to concluding remarks.

II. MODEL AND THEORETICAL APPROACH

We start from the Holstein Hamiltonian

$$H = -\sum_{\langle i,j\rangle,\sigma} J_{ij} c^{\dagger}_{i,\sigma} c_{j,\sigma} + \sum_{j} \sqrt{2} g (n_j - 1) X_j + H_{ph}. \quad (1)$$

The first term describes tunneling of electrons with hopping amplitude J_{ij} between nearest-neighbor sites i and j and the second term couples the displacement X_j of a local oscillator with the electron density $n_j = n_{j,\uparrow} + n_{j,\downarrow}$; $c_{j,\sigma}$ ($c^{\dagger}_{j,\sigma}$) are annihilation (creation) operators for electrons with spin σ on the lattice site j and $H_{ph} = \sum_j \frac{\Omega}{2}(X_j^2 + P_j^2)$ is the Hamiltonian of the free oscillators at each site (Einstein phonon). Because we have in mind an evolution over several picoseconds in a solid state environment, we also add a coupling to a thermal reservoir, so that electrons can pass energy to variables other than the particular mode X. The bath is included via a dissipative self-energy (see Appendixes A, B, and C).

On a bipartite lattice with sublattices A and B, the model favors a symmetry-broken low-temperature state at half filling, with opposite displacement $\langle X_j \rangle = \pm X_0$ for sites j on the two sublattices, and a gap in the electronic spectrum. We consider the model on an infinitely coordinated Bethe lattice at half filling, which allows for an exact solution within dynamical mean-field theory (DMFT) [38,39]. The noninteracting electronic density of states has a semielliptic shape $D(\epsilon) = \frac{4}{\pi W^2}\sqrt{W^2 - 4\epsilon^2}$ with bandwidth W. One can analyze the dynamics after an excitation in terms of the local displacements $X_j(t)$ and the local electronic Green's function $G_j(t,t')$, which determines the local spectral function $\mathcal{A}_j(\omega,t) = -\frac{1}{\pi}\mathrm{Im}G^R_j(\omega,t)$ and the local distribution function $F_j(\omega,t) = G^<_j(\omega,t)/[2\pi i \mathcal{A}_j(\omega,t)]$. A DMFT solution which enforces a spatially homogeneous order parameter and treats the electron-lattice interaction perturbatively gives coherent order-parameter oscillations after an impulsive electronic excitation, as qualitatively expected from time-dependent GLT [22]. Here, we allow for an arbitrary distribution of X_j and G_j. The nonperturbative solution of the dynamics in this case is facilitated by the following steps (additional details are reported in the Appendixes). (i) Because the relevant phonon timescale $1/\Omega$ is slow compared to the electronic timescale, the exact Keldysh action for the oscillator displacement X_j at a given site j can be replaced by a stochastic equation of motion [40]. The coupling of the oscillator to the electronic density fluctuations is replaced by a damping $-\gamma_j(t)\dot{X}_j(t)$ and a stochastic force $\xi_j(t)$ in the white noise limit $\langle \xi_j(t)\rangle = 0$ and $\langle \xi_j(t)\xi_{j'}(t')\rangle = K_j(t)\delta_{j,j'}\delta(t-t')$ (further details about the derivation of these contributions to the equation of motion can be found in Appendix B and in Ref. [41]). The total force on the oscillator at site j is therefore

$$f_j = -\Omega^2 X_j - \sqrt{2} g \Omega (\langle n_j \rangle - 1) - \gamma_j \dot{X}_j + \sqrt{\Omega}\xi_j, \quad (2)$$

where the first two terms are Hooke's law and the standard mean-field (Ehrenfest) force. The damping constant γ_j and the noise amplitude K_j are determined self-consistently by the retarded and Keldysh components of the local electronic density-density correlation function at site j [40]. (ii) After the phonon is replaced by the stochastic variable X_j, the local electronic Green's function G_j becomes a stochastic quantity itself and one must solve the electron dynamics in the presence of a time-dependent disorder. This is achieved using a nonequilibrium generalization of statistical DMFT [42–44]. For the infinitely coordinated Bethe lattice, this implies that the DMFT hybridization function on a given site is determined by an average over the Green's function on the opposite sublattice (see Appendix A for further comments on nonequilibrium statistical DMFT). In the simulations, we explicitly treat 128 representative sites on the A and B sublattices, which give access on the full distribution of local properties. In order to solve the electron dynamics on timescales which are much longer than the intrinsic electron hopping time, we use a quantum Boltzmann equation consistent with DMFT (see Appendix C for a discussion on the quantum Boltzmann equation) [45]. The simulation of the electron dynamics is done here explicitly because *a priori* it is not clear whether electrons locally thermalize in the disordered state. For example, the exact solution of the disordered Falikov-Kimball model predicts nonergodic behavior if the system remains isolated [46].

III. NUMERICAL SIMULATIONS

In the following, we choose representative parameters, with the noninteracting bandwidth $W = 1$ eV to define the energy scale, $\Omega = 0.05$ eV (bare phonon period $\tau \sim 80$ fs) and $g = 0.1$ eV [corresponding to a dimensionless coupling constant $\lambda = 4g^2/(\Omega W) = 0.8$]. All energies are understood in eV unless otherwise stated. We first analyze the equilibrium properties of the model. To prepare an equilibrium state, we

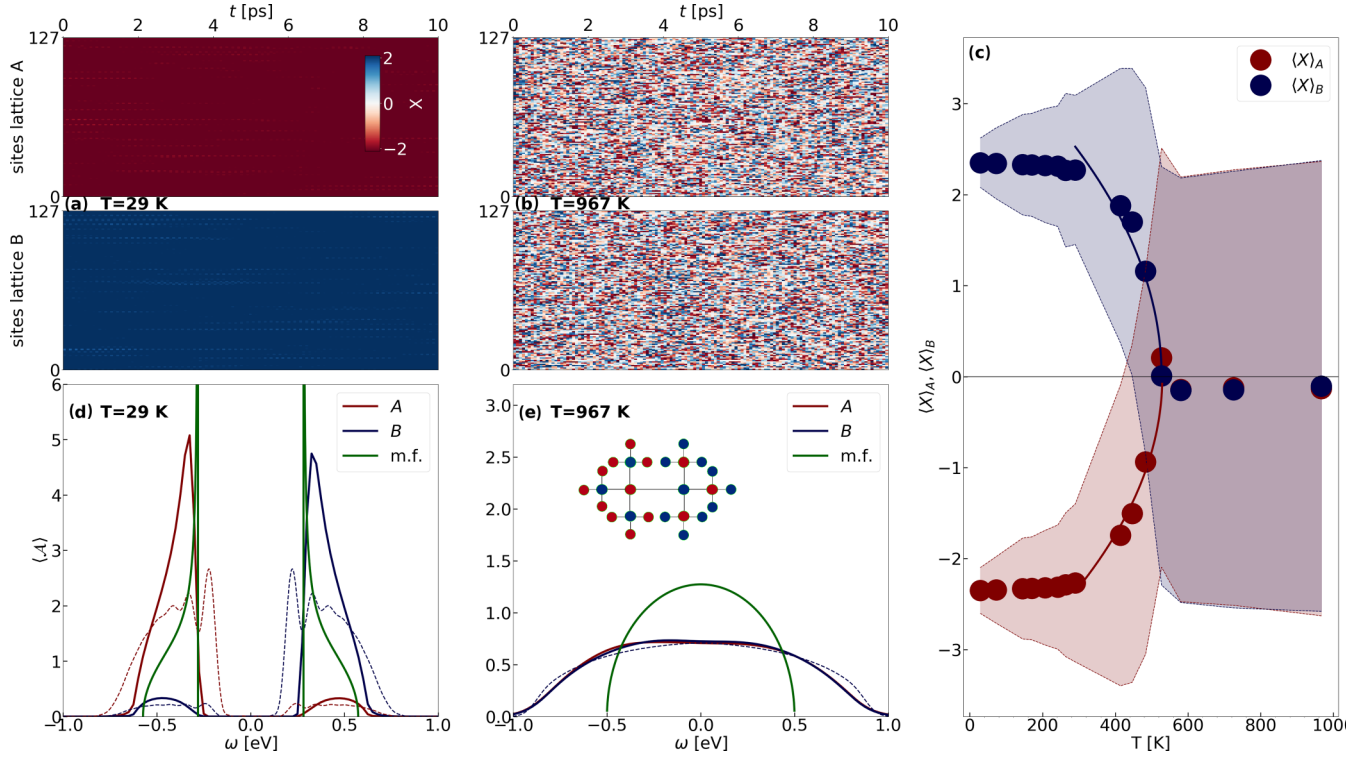

FIG. 1. Equilibrium solution of the model. (a),(b) Stochastic evolution of X_j in the stationary equilibrium phase at a temperature $T = 29$ K corresponding to the ordered phase (a) and at $T = 967$ K in the disordered phase (b). The vertical axis labels the 256 representative sites j, grouping together sites of the same sublattice. Note that there is no correlation between the representative sites; their labeling is arbitrary. (c) Average $\langle X\rangle_\alpha$ for the two sublattices $\alpha = A, B$ as a function of temperature (dots). Solid lines correspond to a fit $\langle X\rangle_{A,B} = \pm C\sqrt{T_c - T}$ in the ordered phase, with $T_c \approx 527$ K. The shaded areas represent the confidence interval of each $\langle X\rangle_\alpha$, with semiamplitude given by the variance $\sigma_\alpha = \sqrt{\langle X^2\rangle_\alpha - \langle X\rangle_\alpha^2}$. $\langle X\rangle_\alpha$ has to be intended as an average over all the $N = 128$ sites in sublattice $\alpha = A, B$ and over all the times: $\langle X\rangle_\alpha \equiv E_t[\frac{1}{N}\sum_{j=1}^{N} X_{j,\alpha}(t)]$, where $E_t[\dots]$ is the expectation value over time. (d),(e) Electronic spectra at $T = 29$ K and $T = 967$ K, respectively. Continuous blue and red lines are the average spectral functions taken over all the impurities belonging to a given sublattice. Green lines show the results of a static mean-field solution with the same order parameter as obtained within the stochastic approach and dashed blue and red lines correspond to the perturbative DMFT solution of Ref. [22] (see discussion). The inset in (e) shows a portion of the Bethe lattice with coordination number 4.

initialize the trajectories with $X_j < 0$ ($X_j > 0$) for $j \in A$ ($j \in B$) and let the system evolve sufficiently long to become stationary on average. Figures 1(a) and 1(b) show the stationary stochastic evolution of the trajectories X_j at all representative sites j at two values of the temperature. At the lower temperature $T = 29$ K [Fig. 1(a)], the system is in the ordered phase, and the displacements on the A and B sublattices fluctuate around nonzero values of opposite sign, $\langle X\rangle_A \approx -2$ and $\langle X\rangle_B \approx 2$. ($\langle\cdot\rangle_\alpha = \langle\cdot\rangle_{j\in\alpha}$ denotes the average over all sites in sublattice $\alpha = A, B$.) At the higher temperature $T = 967$ K [Fig. 1(b)], the system is in the disordered phase, and the displacements at both sublattices fluctuate around $X = 0$. The dependence of the average $\langle X\rangle_A$ and $\langle X\rangle_B$ indicates a second order phase transition at $T_c \approx 527$ K [Fig. 1(c)]. The local electronic density of states $\langle\mathcal{A}(\omega)\rangle_\alpha$ at the two sublattices shows a gap in the ordered phase [Fig. 1(d)], which is closed for $T > T_c$ [Fig. 1(e)]. Both in the ordered and disordered phase, the fluctuations of the displacement imply that the spectra are substantially broadened with respect to a static mean field simulation with a homogeneous order parameter (green solid lines).

Starting from the insulating solution at $T = 145$ K, we now analyze the nonequilibrium dynamics induced by a time-dependent protocol that simulates the photoexcitation of the electrons from the lower to the upper energy band. The transfer of electrons is realized by coupling an electron reservoir with occupied density of states $\mathcal{A}^{<}_{\rm dop}(\omega)$ at positive energies and unoccupied density of states $\mathcal{A}^{>}_{\rm dop}(\omega)$ at negative energies [shaded areas in Fig. 2(a)], for about 3 fs starting at $t = 0$ (see Appendix D for details concerning the excitation protocol). At early times, the average distribution function $\langle F(\omega, t)\rangle_A$ assumes a nonequilibrium shape that cannot be fitted by a Fermi-Dirac function. However, it recovers the original form on a relatively short timescale of about 1 ps. (In the figure, we exemplarily show quantities on sublattice A; quantities on the other sublattice behave analogously.) The early time electron dynamics can be analyzed in terms of the excitation density, given by the integrated occupation at positive frequencies, $n_A^{\rm ex}(t) = \int_0^\infty d\omega\langle F(\omega, t)\mathcal{A}(\omega, t)\rangle_A$ [Fig. 2(b)]. Starting from a peak excitation density of few percent, an almost complete decay of $n_A^{\rm ex}$ due to energy dissipation of the electrons occurs within ~1.3 ps. The average distortion $\langle X\rangle_A - \langle X\rangle_B$ rapidly collapses to zero after the electronic excitation, with an overshoot that represents a strongly damped coherent dynamics [Fig. 2(b)]. After that, $\langle X\rangle_A - \langle X\rangle_B$ remains close to zero for almost ten

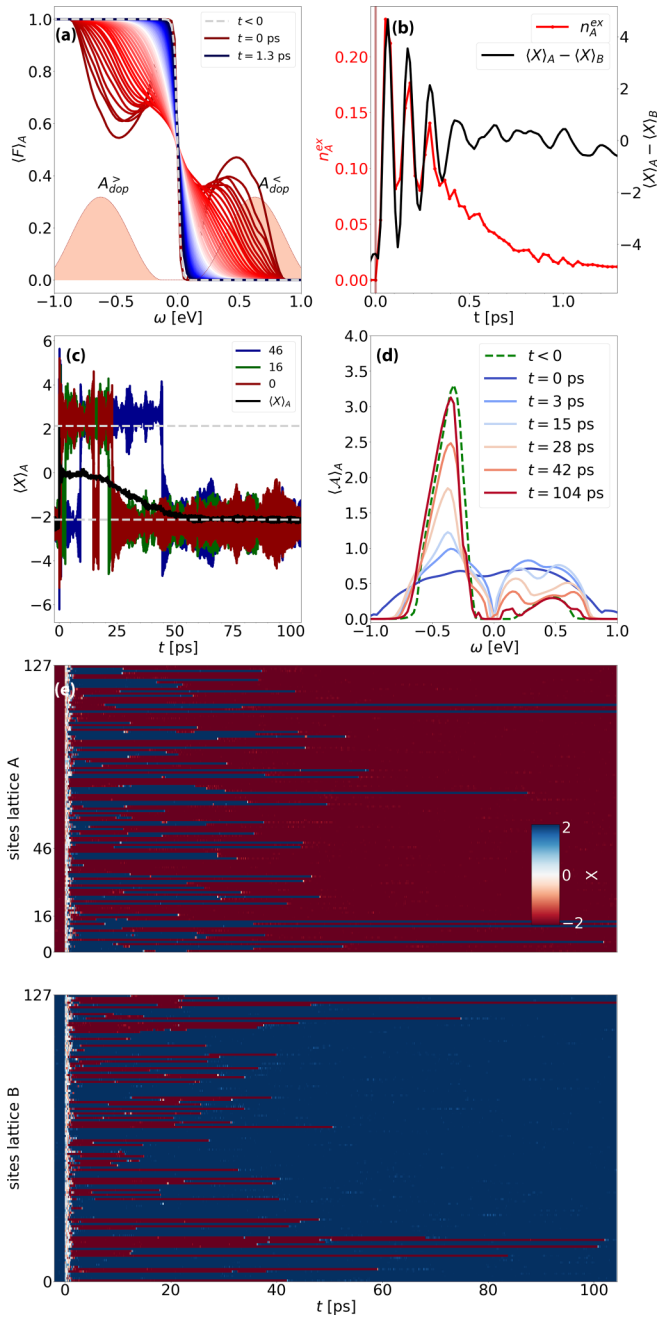

FIG. 2. Nonequilibrium evolution of the system. (a) Time evolution of the electronic distribution function starting from the equilibrium ordered state at $T = 145$ K. The excitation is realized by coupling the system for a period of few fs to a photodoping reservoir with occupied (unoccupied) density of state $\mathcal{A}^{<}_{\rm dop}$ ($\mathcal{A}^{>}_{\rm dop}$) above (below) the Fermi energy (shaded areas). (b) Short time evolution of the difference between the sublattice averages $\langle X\rangle_A - \langle X\rangle_B$ and of the electronic excitation density $n^{\rm ex}_A(t)$. (c) Long time evolution of the average $\langle X\rangle_A$, together with some representative trajectories X_j. (d) Time evolution of the average spectral function $\langle \mathcal{A}(\omega, t)\rangle_A$ for the A sublattice. (e) Time evolution of X_j after the photoexcitation at $t = 0$ for all trajectories.

times the electronic recovery time, up to ∼10 ps [Fig. 3(a)]. For smaller excitation densities, the order parameter is only partially suppressed and subsequently recovers from that value (see Supplemental Material [47]).

The evolution of $\langle X\rangle_A$ on a longer time scale [Fig. 2(c)] reveals a very slow relaxation dynamics. If the order is sufficiently suppressed during the excitation, the final sign of the order parameter becomes random; while the original sign of the order parameter is recovered in the realization shown in Fig. 2(c), other noise realizations can lead to a reverse (see Supplemental Material [47]). The slow dynamics can be linked to the presence of long-living lattice defects, i.e., displacements X_j at specific sites j which assume an opposite value with respect to the average displacement on the sublattice of j. Indeed, even though X_j follows the average $\langle X\rangle_A$ for the majority of sites $j \in A$, a few sites behave differently [see curves $j = 0$, $j = 16$, and $j = 46$ in Fig. 2(c)]. Due to the stochastic nature of the time evolution of the displacements, one can observe trajectories that flip back and forth from positive to negative values, in particular for the early phase of the dynamics. To measure the defect density, we define $n_{\rm def}$ at a given time by counting the percentage of sites j for which X_j has opposite sign compared to the average $\langle X\rangle_\alpha$ on the given sublattice. Immediately after the photoexcitation, $n_{\rm def}$ grows from zero (in the original equilibrium state) to a value close to 50% as $\langle X\rangle_A$ and $\langle X\rangle_B$ drop to zero [Fig. 3(a)]. Subsequently, $n_{\rm def}$ decreases again, but some defects remain even at the latest time of our simulation ($t \sim 100$ ps). Given the large separation of timescales between the electronic and the lattice recovery, we expect the inclusion of a small electron-electron interaction not to alter significantly the previous picture. A more general discussion of the role of the different parameters on the dynamics of the system can be found in the Supplemental Material [47].

To further interpret the data one can look at the full distribution function $P_\alpha(X)$ of the local displacements X on a given sublattice $\alpha = A, B$, which is shown for various times in Figs. 3(b)–3(e). Because $P_A(X) = P_B(-X)$, we show the symmetrized $P(X) = [P_A(X) + P_B(-X)]/2$. In the initial equilibrium state, $P(X)$ is peaked around the mean order parameter $\langle X\rangle_A \approx -2$ [Fig. 3(b)]. Shortly after the excitation, $P(X)$ first becomes parity symmetric with a broad distribution around $X = 0$ [Fig. 3(c)]. During the relaxation, the distribution then develops into a well-defined bimodal form, which is still parity invariant, but has reduced weight at $X = 0$ [Fig. 3(d)]. This bimodal distribution is the hallmark of the inhomogeneously disordered state. At longer times, the asymmetric equilibrium distribution recovers through a gradual depletion of the minority peak [Fig. 3(e)].

The evolution of the lattice displacements is indirectly reflected in the spectral function, which can be observed, e.g., in photoemission spectroscopy. The initial reduction of $\langle X\rangle_A$ leads to rapid closing of the energy gap in the original spectral function $\langle \mathcal{A}(\omega, t)\rangle_\alpha$; see curve for time $t = 0.5$ ps in Figs. 3(f) and 3(g) for the A and B sublattices, respectively. After the recovery of the nonzero average lattice displacements, the gap is partly restored. However, the presence of the defects leads to incoherent spectral weight in the gap, which remains visible even for the longest simulation time $t = 100$ ps [Fig. 2(d)].

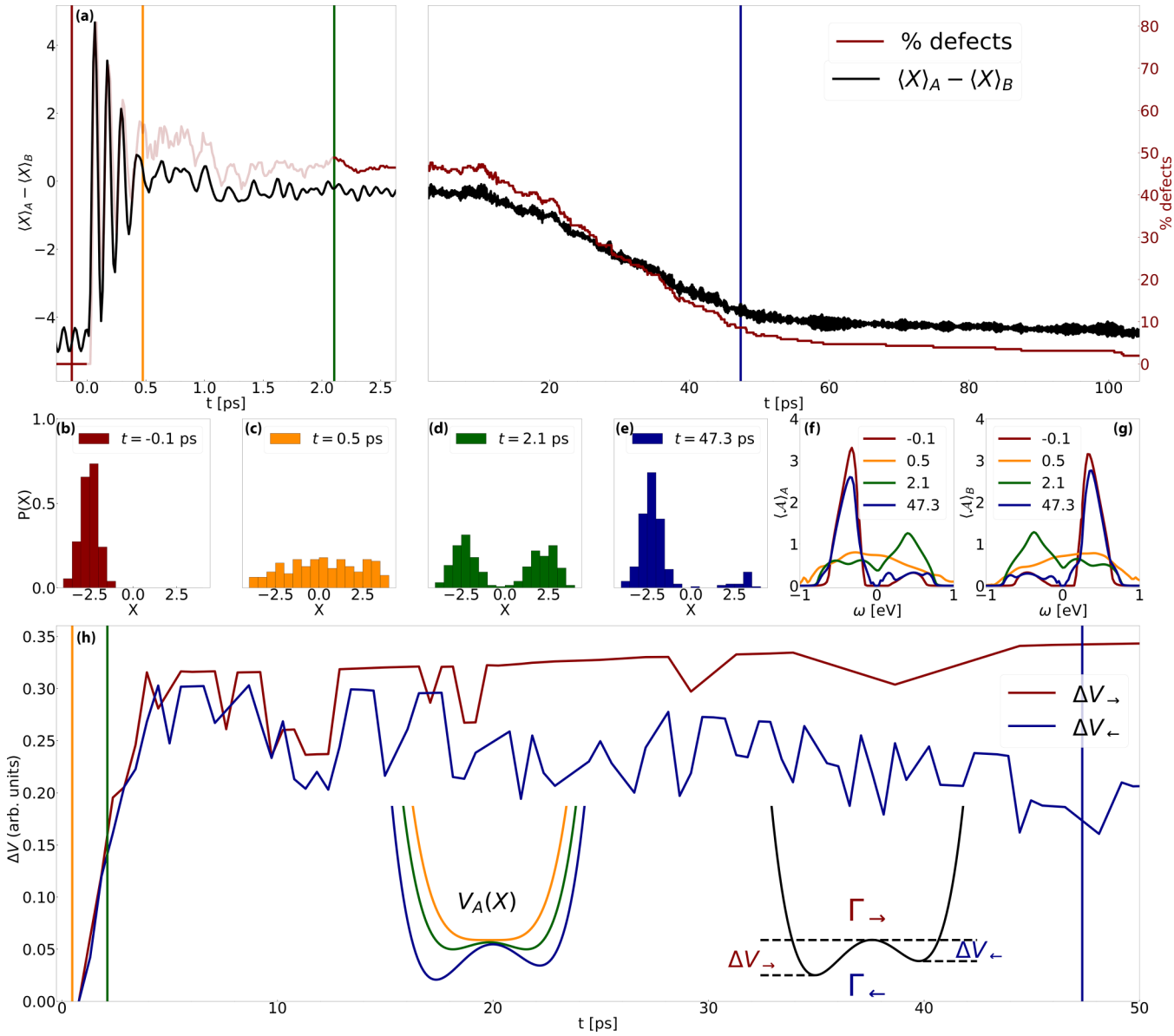

FIG. 3. Characterization of the nonequilibrium dynamics. (a) Early and long times dynamics (left and right panels, respectively) of $\langle X\rangle_A - \langle X\rangle_B$ and of the defect density $n_{\rm def}$, normalized to the total number N_T of A and B lattice sites. (b)–(e) Distribution function of the displacements at different times, as indicated by the vertical lines in panel (a). (f),(g) Local electronic spectral functions for the A and B sublattices, respectively, at the same times as panels (b)–(e). (h) Time evolution of the activation energy from the minority to the majority minimum and back. The left inset shows a sketch of the sublattice potential $V_A(X)$ at different stages of the dynamics as indicated by the vertical lines. The right inset sketches the rates $\Gamma_{\rightarrow}$ ($\Gamma_{\leftarrow}$) for the transition from minority to majority (majority to minority) displacements; $\Delta V_{\rightarrow(\leftarrow)}$ are the barrier heights for the transitions in the two directions.

IV. NONEQUILIBRIUM POTENTIAL ENERGY BARRIER

The long lifetime of the defects suggests that they are protected by an energy barrier in the effective potential $V_\alpha(X)$, which describes the local dynamics of X on sublattice α. For late times, when $P(X)$ shows a bimodal form, we can assume that $V_\alpha(X)$ is represented by a double well with minima for the majority and minority displacements [see right inset in Fig. 3(h)]. One can try to estimate these barriers from the stochastic dynamics, assuming that the rates $\Gamma_{\rightarrow}$ ($\Gamma_{\leftarrow}$) for the transition from minority to majority (majority to minority) are given by the Arrhenius law $\Gamma_{\leftarrow(\rightarrow)} = \Gamma_0 e^{-\Delta V_{\leftarrow(\rightarrow)}/T}$. The barrier heights $\Delta V_{\leftarrow(\rightarrow)}$ for the transitions in the two directions are shown in Fig. 3(h) (see Appendix E for the extraction of the barriers). The dynamics of the energy barriers is characterized by two stages. Up to a time $t \approx 5$ ps before the symmetry breaking sets in, the potential is given by a symmetric double well ($\Delta V_{\leftarrow} = \Delta V_{\rightarrow}$), whose barrier increases almost linearly with time. Once the symmetry is broken, the barrier $\Delta V_{\leftarrow}$ protecting the minority sites remains intact (even if it slowly decreases), but it is now lower than the barrier for the other direction ($\Delta V_{\leftarrow} < \Delta V_{\rightarrow}$), supporting the metastable character of the defects.

An important question is the validity of the white noise approximation made in our simulation. At equilibrium, we can compare our results to a DMFT simulation which treats the electron phonon in leading order perturbation theory but keeps the full retardation effects [22]. In the high-temperature phase, where the displacements fluctuate around $X = 0$, this approach agrees remarkably well with the present simulation regarding the broadening of the equilibrium spectra [see dashed line in Fig. 1(e)]. However, the weak coupling description cannot reproduce the bimodal phonon distribution by construction and is blind to the inhomogeneous disordering, which sets in in the nonequilibrium state. An exact solution of the Holstein model in DMFT is possible in equilibrium using quantum Monte Carlo (QMC) techniques [48,49]. Above the ordering temperature, QMC has predicted a highly non-Gaussian and even bimodal distribution $P(X)$ for the Hubbard-Holstein model [48]. (Deep in the ordered phase, we expect that the minority displacement in equilibrium has a rather small weight and might be difficult to detect.) While nonequilibrium QMC simulations for the long time dynamics are not possible, our results are clearly in line with these equilibrium findings. Finally, we expect the white noise limit to become systematically better for smaller phonon frequencies. We have performed simulations at a lower $\Omega = 0.005$, corresponding to an oscillation period $\tau \sim 830$ fs (keeping the parameter g^2/Ω fixed, which determines the phase transition in equilibrium). One observes more coherent dynamics at early times (few coherent oscillations of $\langle X\rangle_A$ around $X = 0$ after the excitation) followed by a fast recovery at later times which indicates no bimodal distribution at intermediate times and thus a negligible value of the potential energy barrier in this case (see Supplemental Material [47]).

V. CONCLUSIONS

In conclusion, we have shown that the dynamics in a simple Holstein model for a Peierls charge density wave transition can lead to ultrafast inhomogeneous disordering after photoexcitation, with a bimodal distribution of the local order parameter. Experimental signatures for a transiently disordered state may be found using scattering techniques [23] or, as our model suggests, by means of incoherent spectral weight in the electronic spectra. One might also consider optical experiments which are sensitive to local properties; e.g., if local Raman-active modes are affected by the local order parameter, one could map the order parameter distribution onto a nontrivial distribution of frequencies [50] in a stimulated Raman measurement. The stabilization of the disorder is understood in terms of metastable defects, which are local in nature and therefore different from the topologically stabilized defects in the Kibble-Zurek mechanism. The occurrence of inhomogeneous disordering already in the simple Holstein model suggests this phenomenon should be relevant to photoinduced dynamics in solids more generally. In more complex systems, the inhomogeneous disorder at short times might be a step towards true metastability and glassy states at long times [51]. Future theoretical studies will extend the technique developed in this work, i.e., nonequilibrium statistical DMFT with a stochastic lattice evolution, to more realistic descriptions of the coupled electron lattice dynamics, such as a model for VO_2 [52].

ACKNOWLEDGMENTS

We thank S. Wall and P. Werner for useful discussions. We acknowledge financial support from the ERC starting Grant No. 716648. The numerical calculations have been performed at the RRZE of the University Erlangen-Nuremberg.

A.P. wrote the nonequilibrium DMFT code and performed the numerical simulations with inputs from F.G. and M.E. All the authors contributed to the derivation of the stochastic semiclassical equations for the lattice displacements. F.G. and M.E. conceived the project and wrote the manuscript.

APPENDIX A: STATISTICAL DMFT

In DMFT, the Hamiltonian (1) is mapped to a set of Anderson-Holstein impurity problems, one for each lattice site j [38]. These models are defined by the action $S_j = S_j^{\rm loc} + S_j^{\rm hyb}$, where $S_j^{\rm loc}$ describes the coupled electronic and lattice degrees of freedom at the isolated site j and $S_j^{\rm hyb} = \sum_\sigma \int_{\mathcal{C}} dt\, dt' c^*_{j,\sigma}(t)\Delta_j(t,t')c_{j,\sigma}(t')$ is the hybridization of the electrons with a self-consistent environment defined through the hybridization function Δ_j. The action is formulated on the Keldysh time contour $\mathcal{C}$ to describe real-time dynamics (see Refs. [39,40] for an introduction to the Keldysh formalism). On the Bethe lattice with coordination number $Z \to \infty$ and nearest neighbor hopping $J_0/\sqrt{Z}$, Δ_j is given by the average of the local Green's functions G_m at all neighbor sites m of j, $\Delta_j(t,t') = |J_0|^2 \sum_{m\in NN(j)} G_m(t,t')/Z$ [38]. In the present case, we allow all sites to be inequivalent due to a stochastic displacement of the phonons (see below). For $Z \to \infty$ the sum over nearest neighbors of a site j on the A (B) sublattice can be replaced by a statistical average of the respective quantity on the opposite sublattice B (A), so that $\Delta_{A(B)}(t,t') = |J_0|^2\langle G_j(t,t')\rangle_{B(A)}$; $|J_0| = W/4$ is the quarter bandwidth of the noninteracting density of states. In the simulation, we keep 128 representative impurity models (representative sites) for each sublattice and evaluate the statistical average accordingly.

APPENDIX B: STOCHASTIC EQUATION FOR THE LATTICE DISTORTION

To solve the impurity model, we separate its action as $S_j = S^c + S^{cx}$, where S^c contains all purely electronic terms (local contributions and hybridization), and

$$S_j^{cx} = -\int_{\mathcal{C}} dt\, X_j\left[\frac{\left(\partial_t^2 + \Omega^2\right)}{2\Omega}X_j + \sqrt{2}g(n_j - 1)\right] \tag{B1}$$

is the Keldysh action for the displacement X_j. The latter describes the uncoupled dynamics of X_j and the coupling to the density $n_j = \sum_\sigma c^*_{j\sigma}c_{j\sigma}$. To find an effective equation of motion for X_j which still takes into account the electronic fluctuations, we closely follow Ref. [40] for the derivation of the Langevin equation for a damped harmonic oscillator: the electrons are integrated out to obtain an action of X_j only, X_j is separated into "classical" and

"quantum" components $X_j^{\rm cl}$ and $X_j^{\rm q}$, and quadratic fluctuations in $X_j^{\rm q}$ are eliminated in favor of a Gaussian noise through a Hubbard-Stratonovich transformation. The white noise limit is taken because electronic timescales are much faster than the phonon dynamics. In summary, this leads to the following description for the coupled electron-lattice dynamics. (i) The local electronic Green's function $G_j(t,t') = -i\langle T_C c_{j\sigma}(t) c^\dagger_{j\sigma}(t')\rangle_{S_j}$ and the connected electronic density correlation function $\Pi_j(t,t') = i\langle T_C n(t) n(t')\rangle^{\rm con}_{S_j} = iG_j(t,t')G_j(t',t)$ are determined by the impurity action for which X_j is replaced by the time-dependent $X_j^{\rm cl}(t)$. (ii) $X_j^{\rm cl}(t)$ is determined by the equation of motion $\ddot{X}_j^{\rm cl} = f_j$, with the stochastic force Eq. (2). (In the main text, we denote $X_j^{\rm cl} \equiv X_j$ for simplicity.) The coefficients γ_j and K_j in f_j are related to the electronic density correlation function Π_j through $\gamma_j(t) = 2g^2\Omega\,{\rm Im}[\partial_\omega \Pi_j^R(\omega,t)]|_{\omega=0} + \gamma_{\rm HO}$ and $K_j(t) = g^2\Omega\,{\rm Im}[\Pi_j^K(\omega,t)]|_{\omega=0} + 2T\gamma_{\rm HO}$; here $\Pi_j^R(\omega,t)$ $[\Pi_j^K(\omega,t)]$ are the Wigner transform of the retarded (Keldysh) component of Π_j. In the expressions, we have also added a weak extrinsic phonon damping $\gamma_{\rm HO} \sim \frac{1}{26.33}$ ps^{-1} and a consistent noise term $2T\gamma_{\rm HO}$, which accounts for external dissipation to a bath at the initial temperature T. A more detailed derivation of these equations in a more general context can be found in Ref. [41], which as a benchmark also shows that the stochastic semiclassical approach can accurately reproduce the phonon distributions in the thermally disordered phase over a wide parameter regime, compared to numerically exact quantum Monte Carlo simulations.

APPENDIX C: QUANTUM BOLTZMANN EQUATION

After the quantum phonon is replaced with a classical stochastic one, one still has to solve the electron impurity model with a time-dependent term $\propto X_j^{\rm cl}(t) n_j$. The time evolution of the electronic system, on each lattice site, is provided by a quantum Boltzmann equation (QBE) for the local energy distribution function $F_j(\omega,t) = G_j^<(\omega,t)/[2\pi i \mathcal{A}_j(\omega,t)]$ [45]. The QBE gives an equation $\partial_t F_j(\omega,t) = I_{j,\omega}[F]$ for the evolution of the distribution, with scattering integral:

$$I_{j,\omega}[F] = -i\Gamma_j^<(\omega,t) - F_j(\omega,t) 2i\,{\rm Im}\,\Gamma_j^R(\omega,t), \qquad \text{(C1)}$$

where $\Gamma_j(\omega,t) = \Sigma_j(\omega,t) + \Delta_j(\omega,t)$. The self-energy $\Sigma_j(\omega,t)$ in particular incorporates the coupling between the local electronic system and a bosonic bath, which acts as a heat reservoir. In time, $\Sigma_j(t,t') = g_{\rm ph}^2 G_j(t,t') D_{\rm ph}(t,t')$, where $D_{\rm ph}(t,t')$ is the propagator for noninteracting bosons with Ohmic density of states $\frac{\omega}{4\omega_{\rm ph}^2}\exp(-\omega/\omega_{\rm ph})$, $\omega_{\rm ph} = 0.05$, and $g_{\rm ph} = 0.085$ [53,54]. As the coupling to the bath is treated in the weak-coupling formalism, a non-Ohmic bosonic bath should lead to the same qualitative picture presented in the text [55,56], i.e., a cooling of the photoexcited carriers.

APPENDIX D: EXCITATION PROTOCOL

In order to simulate a photodoping excitation, the system is shortly coupled with a fermionic bath with density of states

$$\mathcal{A}_{\rm dop}(\omega) = \mathcal{A}(\omega - 0.625) + \mathcal{A}(\omega + 0.625) \qquad \text{(D1)}$$

consisting of two smooth bands with bandwidth $W_{\rm bath} = 1$ around the energies $\omega_0 = \pm 0.625$. We choose $\mathcal{A}(\omega) = \frac{1}{\pi}\cos^2(\pi\omega/W_{\rm bath})$ in the interval $[\omega_0 - W_{\rm bath}/2, \omega_0 + W_{\rm bath}/2]$. The occupied and unoccupied density of states have spectral shapes given by $\mathcal{A}_{\rm dop}^<(\omega) = \mathcal{A}(\omega - \omega_0)$ and $\mathcal{A}_{\rm dop}^>(\omega) = \mathcal{A}(\omega + \omega_0)$, respectively [shaded areas in Fig. 2(a)]. This fermionic bath adds a local contribution to the electronic self-energy in Eq. (C1), given by $\Sigma_{\rm dop}^{>(<)}(t,\omega) = (-)2\pi i V^2(t)\mathcal{A}_{\rm dop}^{>(<)}(\omega)$, with time-dependent profile $V(t) = V_0 \sin^2(\pi t/t_0)\theta(t)\theta(t_0 - t)$, where $V_0 = 0.125$ (which is a function of the fluence of the pulse) and $t_0 \sim 2.63$ fs (representing the pulse duration). The same excitation protocol has been already applied in [45,57]. Moreover, the fermion bath coupling can be understood as a microscopic model for laser excitation of electrons to/from higher lying bands via dipolar transition matrix elements [58,59].

APPENDIX E: DETERMINATION OF THE ENERGY BARRIERS

To extract the energy barrier ΔV in Fig. 3(h) from the rates $\Gamma_{\rightarrow(\leftarrow)}$ and the Arrhenius law, the constant Γ_0 has been fixed by assuming that the barrier vanishes directly after the excitation, at $t = 500$ fs [Fig. 3(c)]; T is taken to be the final value $T = 145$ K for simplicity because electronic distributions quickly relax as shown in Fig. 2(b). To obtain the rate $\Gamma_\leftarrow$ $(\Gamma_\rightarrow)$ up to a global factor, we measure, over time intervals of $\Delta t = 526$ fs, the average number $n_{\rm maj}$ and $n_{\rm min}$ of majority and minority trajectories, as well as the number of flips $\Delta n_\leftarrow$ and $\Delta n_\rightarrow$ in the two directions. A trajectory is considered as flipped when it previously has been at $X < -1.5$ and arrives at $X > 1.5$ and vice versa. With this $\Gamma_\leftarrow \propto \Delta n_\leftarrow/n_{\rm maj}$ and $\Gamma_\rightarrow \propto \Delta n_\rightarrow/n_{\rm min}$.

[1] D. N. Basov, R. D. Averitt, and D. Hsieh, Nat. Mater. **16**, 1077 (2017).

[2] A. de la Torre, D. M. Kennes, M. Claassen, S. Gerber, J. W. McIver, and M. A. Sentef, Rev. Mod. Phys. **93**, 041002 (2021).

[3] R. Yusupov, T. Mertelj, V. V. Kabanov, S. Brazovskii, P. Kusar, J.-H. Chu, I. R. Fisher, and D. Mihailovic, Nat. Phys. **6**, 681 (2010).

[4] H. Schäfer, V. V. Kabanov, M. Beyer, K. Biljakovic, and J. Demsar, Phys. Rev. Lett. **105**, 066402 (2010).

[5] M. Trigo, P. Giraldo-Gallo, M. E. Kozina, T. Henighan, M. P. Jiang, H. Liu, J. N. Clark, M. Chollet, J. M. Glownia, D. Zhu *et al.*, Phys. Rev. B **99**, 104111 (2019).

[6] T. Huber, S. O. Mariager, A. Ferrer, H. Schäfer, J. A. Johnson, S. Grübel, A. Lübcke, L. Huber, T. Kubacka, C. Dornes *et al.*, Phys. Rev. Lett. **113**, 026401 (2014).

[7] M. J. Neugebauer, T. Huber, M. Savoini, E. Abreu, V. Esposito, M. Kubli, L. Rettig, E. Bothschafter, S. Grübel, T. Kubacka, J. Rittmann, G. Ingold, P. Beaud, D. Dominko, J. Demsar, and S. L. Johnson, Phys. Rev. B **99**, 220302(R) (2019).

[8] P. Beaud, A. Caviezel, S. O. Mariager, L. Rettig, G. Ingold, C. Dornes, S.-W. Huang, J. A. Johnson, M. Radovic, T. Huber *et al.*, Nat. Mater. **13**, 923 (2014).

[9] A. Zong, P. E. Dolgirev, A. Kogar, E. Ergeçen, M. B. Yilmaz, Y.-Q. Bie, T. Rohwer, I.-C. Tung, J. Straquadine, X. Wang, Y. Yang, X. Shen, R. Li, J. Yang, S. Park, M. C. Hoffmann, B. K. Ofori-Okai, M. E. Kozina, H. Wen, X. Wang, I. R. Fisher, P. Jarillo-Herrero, and N. Gedik, Phys. Rev. Lett. **123**, 097601 (2019).

[10] H. Ichikawa, S. Nozawa, T. Sato, A. Tomita, K. Ichiyanagi, M. Chollet, L. Guerin, N. Dean, A. Cavalleri, S.-i. Adachi *et al.*, Nat. Mater. **10**, 101 (2011).

[11] L. Stojchevska, I. Vaskivskyi, T. Mertelj, P. Kusar, D. Svetin, S. Brazovskii, and D. Mihailovic, Science **344**, 177 (2014).

[12] M. Budden, T. Gebert, M. Buzzi, G. Jotzu, E. Wang, T. Matsuyama, G. Meier, Y. Laplace, D. Pontiroli, M. Riccò *et al.*, Nat. Phys. **17**, 611 (2021).

[13] J. Maklar, Y. W. Windsor, C. W. Nicholson, M. Puppin, P. Walmsley, V. Esposito, M. Porer, J. Rittmann, D. Leuenberger, M. Kubli *et al.*, Nat. Commun. **12**, 2499 (2021).

[14] A. Zong, P. E. Dolgirev, A. Kogar, Y. Su, X. Shen, J. A. W. Straquadine, X. Wang, D. Luo, M. E. Kozina, A. H. Reid *et al.*, Phys. Rev. Lett. **127**, 227401 (2021).

[15] Z. Sun and A. J. Millis, Phys. Rev. X **10**, 021028 (2020).

[16] P. E. Dolgirev, M. H. Michael, A. Zong, N. Gedik, and E. Demler, Phys. Rev. B **101**, 174306 (2020).

[17] F. Grandi and M. Eckstein, Phys. Rev. B **103**, 245117 (2021).

[18] J. Bauer, M. Babadi, and E. Demler, Phys. Rev. B **92**, 024305 (2015).

[19] Y. Lemonik and A. Mitra, Phys. Rev. B **96**, 104506 (2017).

[20] Y. Lemonik and A. Mitra, Phys. Rev. B **98**, 214514 (2018).

[21] C. Stahl and M. Eckstein, Phys. Rev. B **103**, 035116 (2021).

[22] F. Randi, M. Esposito, F. Giusti, O. Misochko, F. Parmigiani, D. Fausti, and M. Eckstein, Phys. Rev. Lett. **119**, 187403 (2017).

[23] S. Wall, S. Yang, L. Vidas, M. Chollet, J. M. Glownia, M. Kozina, T. Katayama, T. Henighan, M. Jiang, T. A. Miller *et al.*, Science **362**, 572 (2018).

[24] D. Perez-Salinas, A. S. Johnson, D. Prabhakaran, and S. Wall, Nat. Commun. **13**, 238 (2022).

[25] A. S. Johnson, D. Moreno-Mencía, E. B. Amuah, M. Menghini, J.-P. Locquet, C. Giannetti, E. Pastor, and S. E. Wall, Phys. Rev. Lett. **129**, 255701 (2022).

[26] R. Nandkishore and D. A. Huse, Annu. Rev. Condens. Matter Phys. **6**, 15 (2015).

[27] D. A. Abanin, E. Altman, I. Bloch, and M. Serbyn, Rev. Mod. Phys. **91**, 021001 (2019).

[28] G. Carleo, F. Becca, M. Schiró, and M. Fabrizio, Sci. Rep. **2**, 243 (2012).

[29] A. Smith, J. Knolle, R. Moessner, and D. L. Kovrizhin, Phys. Rev. Lett. **119**, 176601 (2017).

[30] N. Y. Yao, C. R. Laumann, J. I. Cirac, M. D. Lukin, and J. E. Moore, Phys. Rev. Lett. **117**, 240601 (2016).

[31] Z. Lan, M. van Horssen, S. Powell, and J. P. Garrahan, Phys. Rev. Lett. **121**, 040603 (2018).

[32] M. van Horssen, E. Levi, and J. P. Garrahan, Phys. Rev. B **92**, 100305(R) (2015).

[33] A. F. Kemper, M. A. Sentef, B. Moritz, J. K. Freericks, and T. P. Devereaux, Phys. Rev. B **92**, 224517 (2015).

[34] M. A. Sentef, A. F. Kemper, A. Georges, and C. Kollath, Phys. Rev. B **93**, 144506 (2016).

[35] P. Werner, N. Tsuji, and M. Eckstein, Phys. Rev. B **86**, 205101 (2012).

[36] N. Tsuji, M. Eckstein, and P. Werner, Phys. Rev. Lett. **110**, 136404 (2013).

[37] H. Seo, Y. Tanaka, and S. Ishihara, Phys. Rev. B **98**, 235150 (2018).

[38] A. Georges, G. Kotliar, W. Krauth, and M. J. Rozenberg, Rev. Mod. Phys. **68**, 13 (1996).

[39] H. Aoki, N. Tsuji, M. Eckstein, M. Kollar, T. Oka, and P. Werner, Rev. Mod. Phys. **86**, 779 (2014).

[40] A. Kamenev, *Field Theory of Non-Equilibrium Systems* (Cambridge University Press, Cambridge, UK, 2011).

[41] A. Picano, F. Grandi, P. Werner, and M. Eckstein, arXiv:2209.00428.

[42] E. Miranda and V. Dobrosavljević, 6 Dynamical mean-field theories of correlation and disorder, in *Conductor-Insulator Quantum Phase Transitions*, edited by V. Dobrosavljevic, N. Trivedi, and J. M. Valles, Jr. (Oxford Academic, online edn, Oxford, 2012), pp. 161–243.

[43] V. Janiš and D. Vollhardt, Phys. Rev. B **46**, 15712 (1992).

[44] V. Dobrosavljević and G. Kotliar, Phys. Rev. Lett. **71**, 3218 (1993).

[45] A. Picano, J. Li, and M. Eckstein, Phys. Rev. B **104**, 085108 (2021).

[46] M. Eckstein and M. Kollar, Phys. Rev. Lett. **100**, 120404 (2008).

[47] See Supplemental Material at http://link.aps.org/supplemental/10.1103/PhysRevB.107.245112 for the analysis of a different parameter regime with respect to what has been analyzed in the main text, for an analysis of the dependence of the dynamics by V_0, t_0, and $g_{\rm ph}$, and for the time evolution of the stochastic noise and the damping.

[48] F. F. Assaad and T. C. Lang, Phys. Rev. B **76**, 035116 (2007).

[49] P. Werner and A. J. Millis, Phys. Rev. Lett. **99**, 146404 (2007).

[50] D. Fausti, O. V. Misochko, and P. H. M. van Loosdrecht, Phys. Rev. B **80**, 161207(R) (2009).

[51] Y. A. Gerasimenko, I. Vaskivskyi, M. Litskevich, J. Ravnik, J. Vodeb, M. Diego, V. Kabanov, and D. Mihailovic, Nat. Mater. **18**, 1078 (2019).

[52] F. Grandi, A. Amaricci, and M. Fabrizio, Phys. Rev. Res. **2**, 013298 (2020).

[53] N. Dasari, J. Li, P. Werner, and M. Eckstein, Phys. Rev. B **103**, L201116 (2021).

[54] F. Grandi, J. Li, and M. Eckstein, Phys. Rev. B **103**, L041110 (2021).

[55] E. Y. Wilner, H. Wang, M. Thoss, and E. Rabani, Phys. Rev. B **92**, 195143 (2015).

[56] F. Peronaci, O. Parcollet, and M. Schiró, Phys. Rev. B **101**, 161101(R) (2020).

[57] J. Li, D. Golez, G. Mazza, A. J. Millis, A. Georges, and M. Eckstein, Phys. Rev. B **101**, 205140 (2020).

[58] P. Werner, M. Eckstein, M. Müller, and G. Refael, Nat. Commun. **10**, 5556 (2019).

[59] F. Grandi and M. Eckstein, arXiv:2104.03644.